Journal of Scientific & Industrial Research
Vol. 67, September 2008, pp. 697-702

Computation of flow in a target flowmeter

Ümit N Temel, Adnan Öztürk and Ali Pinarbasi*

Cumhuriyet University, Engineering Faculty, Mechanical Engineering Department, 58140, Sivas, Turkey

Received 28 May 2007; revised 17 June 2008; accepted 20 June 2008

Present study determines optimum geometry for target fluidic flowmeter capable to function at small Reynolds numbers (<300). Using fluent code solver, numerical studies were carried out for gasoil measurements at various geometries and Reynolds numbers. Computational technique for unsteady incompressible viscous flow applicable to two dimensional flow geometries is presented. Effects of nozzle exit-target distance (Xt) and target width (Wt) were studied to determine optimum geometry. Flow characteristics and oscillation mechanism were investigated for a flowmeter.

Keywords: Target fluidic flowmeter, Reynolds numbers

Introduction

Target fluidic flowmeters (TFLs) have widespread applications in liquid, gas and steam measurement. Computer simulation of TFLs at low Reynolds numbers (Re) has been reported[1]. However, most studies[2,3] were carried out using two dimensional simulation for vortex shedder. Some experimental setup was designed to obtain TFL performance characteristics[4,5]. Since calibrations of TFLs are insensitive to fluid properties, there is a need for obtaining geometry of TFLs for applications where minimum Re are low. Present study determines optimum geometry (OG) for TFLs capable to function at small Re (<300).

Methodology

Important geometrical parameters[4] of TFL (nozzle to target distance, X_t; target to knife edge distance, X_k; knife edge setback from centre line, Y_k; side wall setback, Y_w; profile depth, H_n; and target width, W_t) are normalized with respect to nozzle exit width d_n as

$$x_t = \frac{X_t}{d_n}, x_k = \frac{X_k}{d_n}, y_k = \frac{Y_k}{d_n}, y_w = \frac{Y_w}{d_n}, a_r = \frac{H_n}{d_n}, w_t = \frac{W_t}{d_n} \quad ...(1)$$

In earlier study[4], y_w, y_k and a_r (aspect ratio) were determined as 8, 5 and 5 respectively. In this study, pair of knife edges is fixed at a distance 21 d_n from nozzle exit. Thus, effect of remaining important parameters (x_t and w_t) was studied to determine OG. However, too close or away nozzle-target distance and too narrow or wide target width make TFLs unattractive. Since, at these conditions, unsteady flow phenomena disappear and flow oscillations cannot be obtained. For these reasons, optimum range for nozzle-target distance and target width are reported[4] as $9 \le x_t \le 13$ and $1.5 \le w_t \le 2$ respectively. In this study, six different geometries (three different x_t as 9, 11, 13 with two different target widths as 1.5 and 2 for each x_t distances) were investigated.

Numerical Procedure

Verification of computer simulation on flow geometry is carried out using available experimental data. In this study, six different geometries of TFL have been described as dimensionless form by using fluent package programs (Table 1, Fig. 1). For numerical solution, fluid domain must be divided into subdivision, resulting in total of 18,000-19,000 unstructured triangular computational cells generated. Mesh structure for one of six geometries (Geometry 1: x_t=9; w_t=1.5; y_k=5) is shown in Fig. 2a. Smaller grid is used in the region between target and edges (Fig. 2b) to improve computational accuracy. Grid density is higher than that of in other region.

2-D unsteady Navier-Stokes equations were solved by means of a commercial CFD package FLUENT based on finite volume method, with an assumption laminar,

*Author for correspondence
E-mail: alipinarbasi@cumhuriyet.edu.tr

Table 1—Geometrical parameters

Geometry	X_t/d	W_t/d	Y_k/d	Y_w/d	X_k/d
1	9	1.5	5	8.5	12
2	9	2	5	8.5	12
3	11	1.5	5	8.5	10
4	11	2	5	8.5	10
5	13	1.5	5	8.5	8
6	13	2	5	8.5	8

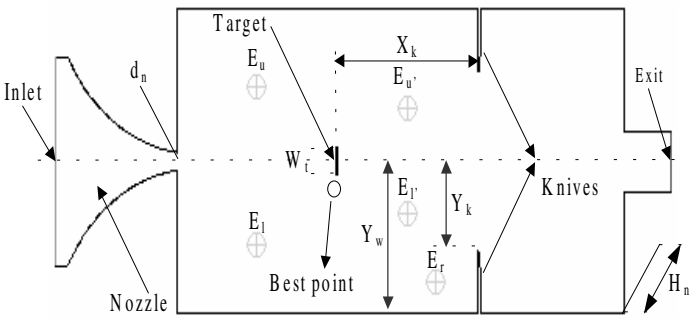


Fig. 1—Schematic diagram of target fluidic flowmeter

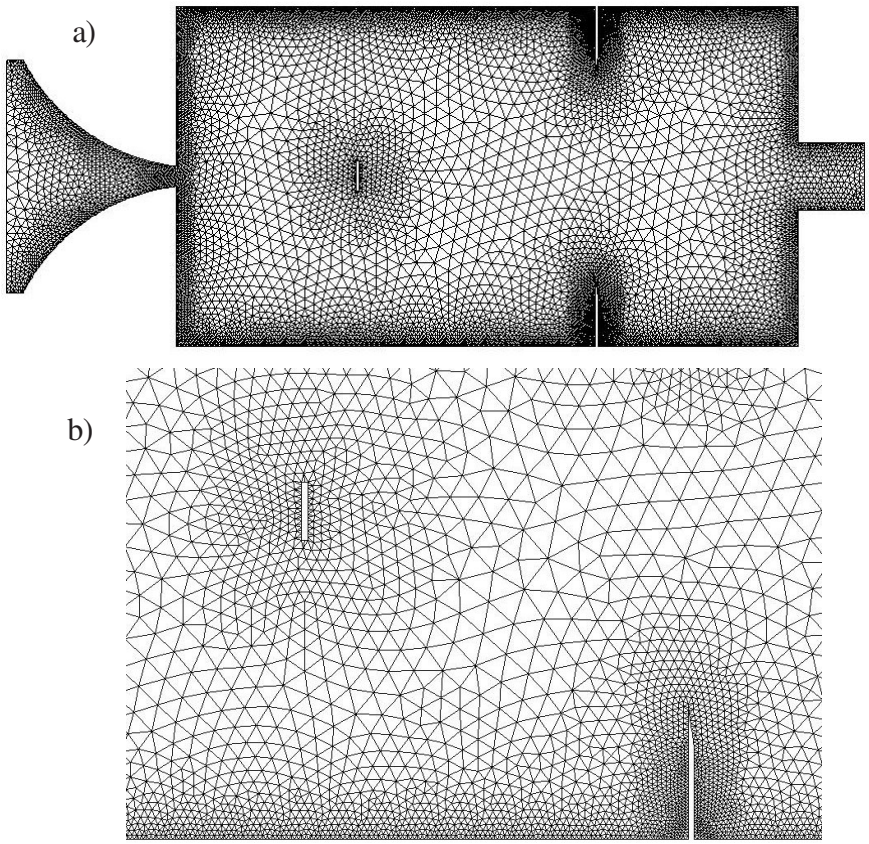


Fig. 2—a) Unstructured mesh for the numeric simulations (for geometry 1 x_t=9,w_t=1.5,y_k=5); b) grid distribution

incompressible and Newtonian flow. Governing u and v momentum equations are integrated on each control volumes to construct algebraic equations. Linearization of these equations and solution (by means of iterative method) of resultant linear equation system yield updated values of dependent variables (pressure and velocity field). Since obtained velocities may not satisfy continuity equation locally, so a Poisson-type equation for pressure correction was derived from continuity equation and linearized momentum equations. This pressure equation is then solved to get necessary corrections to pressure and velocity fields in order to satisfy continuity condition. Iterations are carried out till convergence of solution. In this study, walls were rigid with no slip conditions. At inlet boundary, fully developed axial velocity profiles calculated for flow inside TFL passage. A constant pressure boundary was imposed at outlet, which was placed sufficiently far from target

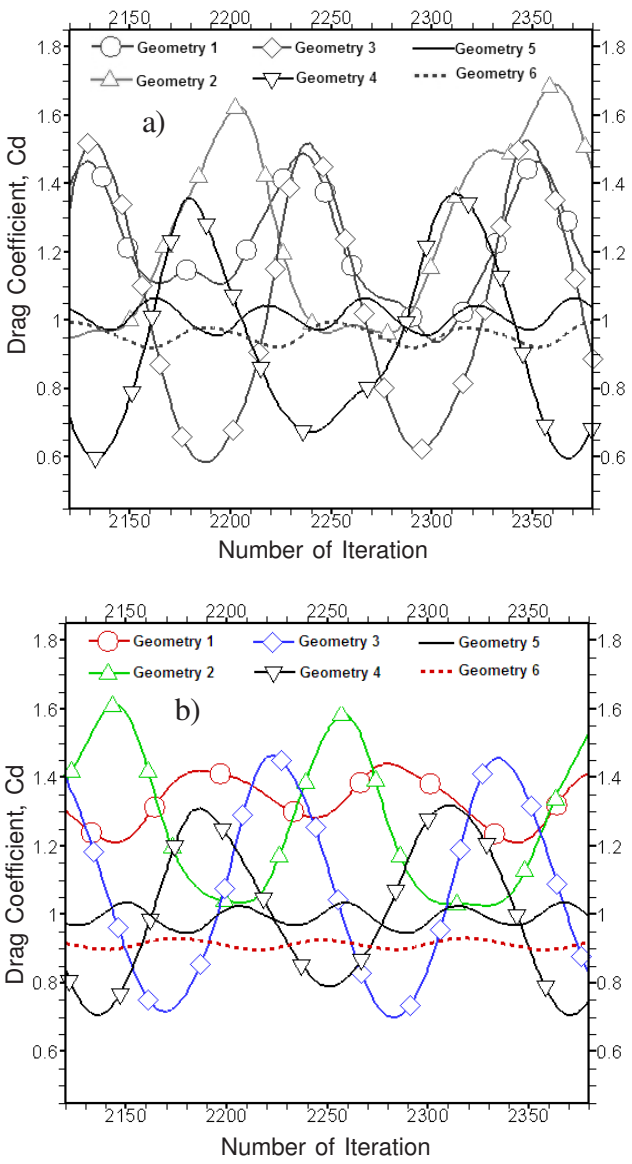


Fig. 3—Drag coefficient distributions for flowmeter models a) For Re 300; b) For Re 200

section. Quadratic upwind differencing (QUICK) scheme was employed for all equations with simple velocity–pressure coupling algorithm in CFD calculations.

Results and Discussion

Optimum Geometry (OG)

To determine OG, numerical solutions were carried for various Re (<300) and TFL performance characteristics were taken as: i) Minimum Re for flow oscillation and flow rate measurement; ii) Quality of oscillation signal to determine flow frequency; and iii) Matching maximum flow oscillations for all geometries at best measuring location[6]. After numerical solutions, main jet impacting on target got split into upper and lower jets. Periodic flow variations are achieved between upper side and lower side after iterations for all geometries. Variation of drag coefficients (DCs) for one period is "m" shaped. When flow passes upper or lower side, DC values are minimum, whereas when jet passes through target center, DC values are maximum. Re is given as

$$\mathrm{Re} = \frac{u_n d_n}{\nu} \qquad \ldots(2)$$

where, u_n, averaged flow velocity at nozzle exit; d_n, width of nozzle exit; ν, kinematic viscosity.

Based on signal quality, amplitude and smoothness of DC oscillations may be compared (Fig. 3). It is said that amplitude of oscillations decreases with reduction of Re. Generally, for same Re, oscillation amplitude of geometry 3 is larger than other geometries, leading to OG (Table 2). Best sinusoidal variations are obtained for geometry 3 and geometry 6 in relation with smoothness of oscillation. Geometry 6 was not found OG based on minimum Re. Therefore, based on signal quality, geometry 3 is considered as OG.

Another criterion for OG is matching maximum flow (U_x, velocity in x direction) oscillations for all geometries at best measuring location[6] (Fig. 1). Amplitude of oscillations decreases on reduction of Re. Higher amplitudes of flow oscillation can be obtained for geometry 3 at same Re (Fig. 4), resulting into OG. Strouhal number (St) as a dimensionless form of flow frequency is expressed as

$$\mathrm{St} = \frac{f d_n}{u_n} = \frac{d_n}{T u_n} \qquad \ldots(3)$$

where f, frequency of flow oscillation; d_n, width of nozzle exit; u_n, flow velocity at nozzle exit; T, oscillation period.

Unsteady numerical solutions were carried out to obtain St–Re variations for Re<300. For these geometries, matching one periodic velocity contour determines periods of flow and then St was calculated. Performance characteristic of TFL was measured in terms of St-Re variation for four geometries (Fig. 5). It is desired that St–Re calibration must be constant or at least smoothly varying. Geometry 3 has been found with least variation among all geometries (Fig. 5). Generally, magnitudes of St in geometry 3 are more than that of others. As a result of unsteady numerical solutions, it is also said that geometry 3 is OG based on St–Re variations.

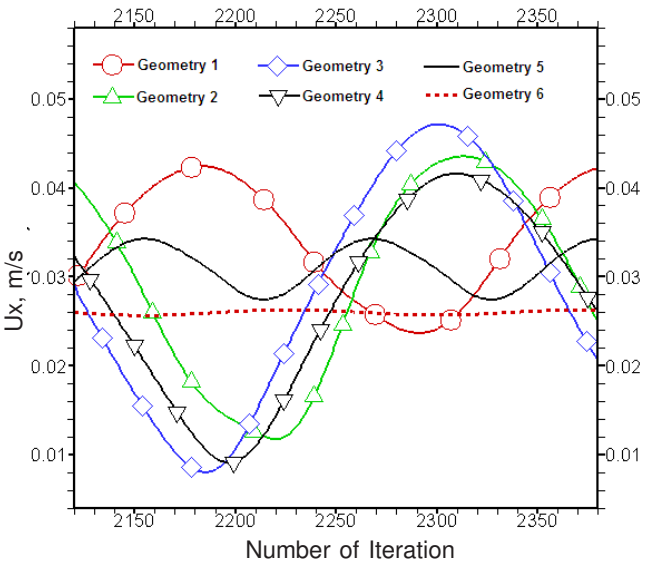


Fig. 4—U_x velocity variation for Re 150

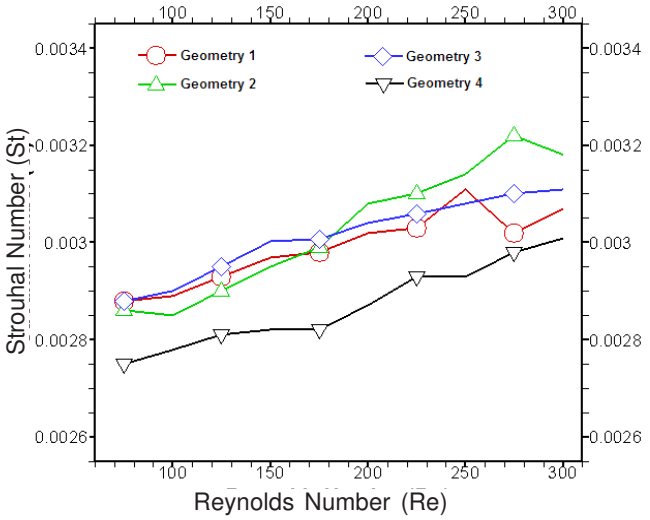


Fig. 5—Strouhal number – Reynolds number variation

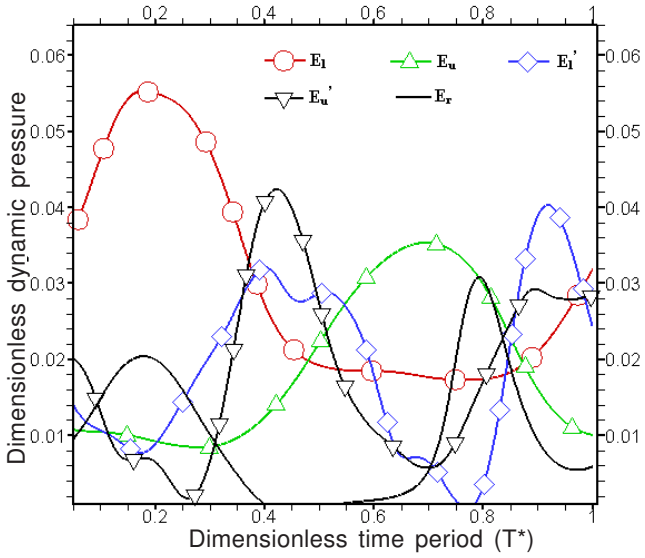


Fig. 6—Dimensionless dynamic pressures at various locations

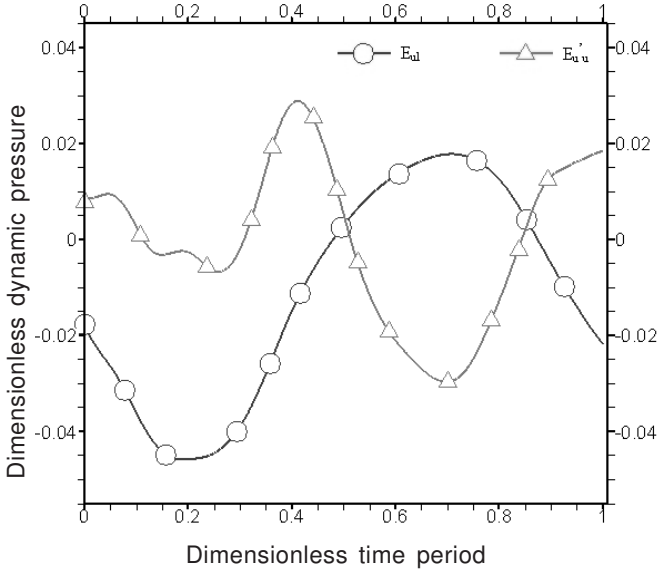


Fig. 7—Variation of E_{ul} and $E_{u'u}$ with T

Table 2—Amplitude of drag coefficients

Drag Coefficient, Cd	Re	Geometry					
		1	2	3	4	5	6
	300	0.5379	0.7354	0.9311	0.7616	0.1072	0.0731
	275	0.4993	0.6959	0.9026	0.7468	0.1051	0.0653
	250	0.3448	0.6231	0.8781	0.7298	0.1002	0.0528
	225	0.2707	0.6109	0.8147	0.6786	0.0949	0.0448
	200	0.2286	0.5778	0.7517	0.6045	0.082	0.0327
	175	0.1973	0.4983	0.6599	0.4638	0.0733	0.0151
	150	0.179	0.3695	0.5419	0.3117	0.0558	0.0011
	125	0.1499	0.2626	0.3724	0.1885	0.0213	0
	100	0.0989	0.2053	0.1538	0.1297	0	0
	75	0.0346	0.1283	0.0188	0.0325	0	0

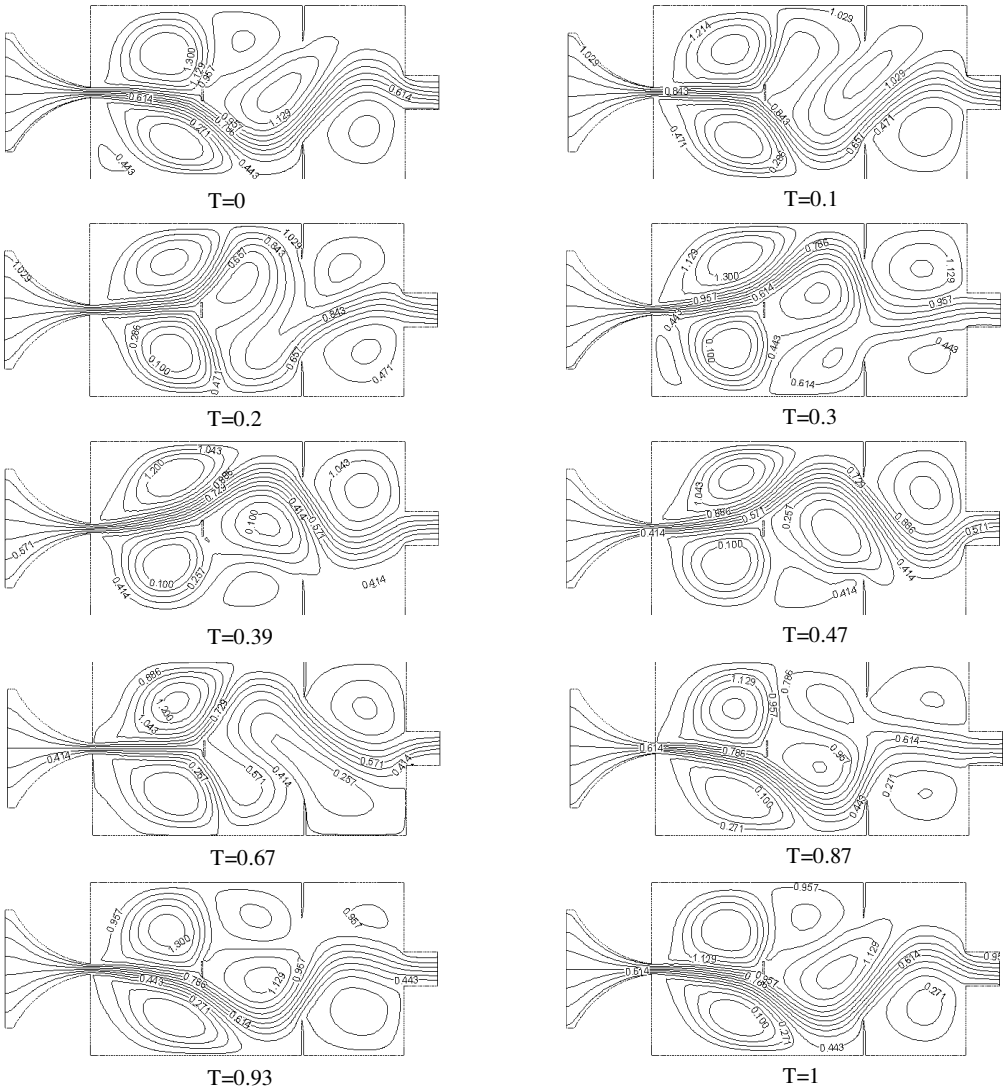


Fig. 8—Computed flow streamlines in the target fluidic flowmeter for one oscillation cycle at Re 150

Dynamic Pressure Distributions and Streamlines

Dimensionless dynamic pressure distribution at different locations (Fig. 1) was obtained for one dimensionless time period. Normalization is relative to nozzle dynamic head ($\frac{1}{2}\rho u_n^2$).

$$E_u = \frac{P_u}{\frac{1}{2}\rho u_n^2}, \quad E_r = \frac{P_r}{\frac{1}{2}\rho u_n^2} \quad E_{ul} = \frac{P_u - P_l}{\frac{1}{2}\rho u_n^2}, \quad E_{u'u} = \frac{P_{u'} - P_u}{\frac{1}{2}\rho u_n^2}, \quad E_{u'} = \frac{P_l - P_{l'}}{\frac{1}{2}\rho u_n^2} \qquad \ldots(4)$$

where, $E_{u,}$ Dimensionless dynamic pressure at upper front region of target; E_r, Dimensionless dynamic pressure at lower knife front; E_{ul}, Dimensionless dynamic pressures difference between upper front region of target and lower front region of target; $E_{u'u}$, Dimensionless dynamic pressures difference between upper back region of target and upper front region of target; $E_{ll'}$ Dimensionless dynamic pressures difference between lower front region of target and lower back region of target; P_u, Dynamic pressure at upper front region of target; P_l, Dynamic pressure at lower front region of target; $P_{u'}$, Dynamic pressure of upper back region of target; $P_{l'}$, Dynamic pressure of lower back region of target; P_r, Dynamic pressure of lower knife front; Á, Density of gasoil.

Dimensionless time period (T^*) is obtained between certain initial time (t_i) and final time (t_f) as

$$T^* = \frac{t_i - t_f}{T} \qquad \ldots(5)$$

Analysis of dynamic pressure distributions shows that for $0 \le T^* \le 0.18$, deflection of lower secondary jet (S_l) onto lower knife edge diverts flow into recirculation region

beneath main jet, so E_l rises whereas E_u decreases slowly (Fig. 6). In this case, E_{ul} decreases (Fig. 7) and main jet deflects upward (Fig. 8). Lower knife front pressure (E_r) increases because of flow directed to knife. While S_l decreases as lower jet deflection angle θ_l increases, and upper secondary jet (S_u) begins to rise as upper jet deflection angle θ_u decreases. At T^*=0.18, jet acts to target along geometric centre line and flow creates symmetrical patterns. For $0.18 \le T^* \le 0.39$, E_l and E_u decreases until T^*= 0.28. After T^*=0.28, E_u begins to rise; but since values of E_l being higher than E_u for $0.18 \le T^* \le 0.39$, E_{ul} decrease initially but increase later (Fig. 7), resulting in upward deflection of main jet. During this period, jet is moving away from centre and S_u deflecting more and more along the target and S_l continue to reduce. At the end of this range (T^*=0.39), S_l reaches to a minimum value. However, on upper side, jet reattachment point becomes closer and closer to knife edge. Thus, adverse pressure gradient, which occurs between upper knife edge and upstream region, causes boundary layer separation and thus reduction in jet curvature.

For $0.39 \le T^* \le 0.47$, absolute value of $E_{u'u}$ is found higher than E_{ul} indicating that $E_{u'u}$ plays important role on flow mechanism. At T^*=0.39, S_u is maximum, then it initiate to reduction. After T^*=0.47, S_l occurs with a higher deflection angle θ_l. For $0.47 \le T \le 0.69$, E_u rises until T^*=0.69 (maximum value) whereas E_l decreases slowly (Fig. 7); also, S_u decreases with θ_u increase, and S_l increases with θ_l decrease. After T^*=0,69, flow structure turns to symmetrical form. For $0.69 \le T^* \le 0.87$, E_u and E_l decrease until T^*=0.77. After T^*=0.77, E_l begins to rise but values of E_u are higher than E_l for $0.69 \le T^* \le 0.87$, resulting deflection of main jet to downward direction. During this period, jet moves away from centre and S_l deflects more and more along target and S_u continue to reduce. However, E_r rises sharply from T^*=0.77 and then adverse pressure gradient occurs between lower knife edge and upstream. This adverse pressure gradient causes reduction in boundary layer separation and jet curvature. At T^*=0.87, $E_l = E_u$. For $0.87 \le T^* \le 0.93$, E_{ul} decreases but $E_{u'u}$ increases. Since value of $E_{u'u}$ is higher than E_{ul}, jet moves towards downward direction. After T^*=0.87, S_l reaches to maximum value. For $0.93 \le T^* \le 1$, rising of $E_{l'l}$ plays important role on mechanism and downward deflection is stopped at T^*=0.93. After T^*=0.93, upward deflection initiates and S_l begins to reduce and S_u rising. At T^*= 1, one period is completed and then same mechanism is repeated.

Conclusions

For determination of optimum geometry, target fluidic flowmeter performance characteristics were considered such as minimum Re (<300), oscillation quality and St-Re variation. Optimum geometry for target flowmeter is determined as the dimension of x_t=11, w_t=1.5, y_k=5 of geometry 3 comparing the minimum Re, oscillation of signal and St–Re variation. Potential core of jet ceases to exist at outlet of nozzle in a confined jet issuing from a rectangular nozzle into a chamber. A feedback loop occurs in two side of target before disappearing through the outlet. Target must be placed in turbulent region for flow oscillation to exist and be regular. Therefore, values of X_t/d ratio must be fixed at 11 (target width for 1.5) for attaining flow rate measurements.

References

1 Fromm J E & Harlow F H, Numerical solution of the problem of vortex street development, *Phys Fluids*, **6** (1963) 975-982.

2 El Wahed A K, Johnson M W & Sproston L, Numerical study of vortex shedding from different shaped bluff bodies, *J Flow Meas Instrum*, **4** (1993) 233-240.

3 Davis R W, Moore E F & Purtell P, A numerical, experimental study of confined flow around rectangular cylinders, *Phys Fluids*, **27** (1984) 46-59.

4 Boucher R F & Mazharoglu C, Low Reynolds number fluidic flow metering, *J Phys E Sci*, **21** (1988) 977-989.

5 Honda S & Yamasaki H, A new hydrodynamic oscillator type flow meter, in *Proc.of Int Symp Fluid Control & Measurement* (Tokyo) 1985.

6 Lua AC & Zheng Z, Numerical simulations and experimental studies on a target fluidic flowmeter, *J Flow Meas Instrum*, 14, (2003) 43-49.